1 **Dispersal and attenuation of trace contaminants downstream of the Ajka bauxite**

2 **residue (red mud) depository failure, Hungary**

3

4 William M. Mayes[*1]; Adam P. Jarvis[2]; Ian T. Burke[3]; Melanie Walton[1]; Viktória

5 Feigl[4]; Orsolya Klebercz[4]; Katalin Gruiz[4].

6

7 [*] corresponding author, tel: +44(0)1723357292; fax: +44(0)1723370815; email: W.Mayes@hull.ac.uk

8 [1] Centre for Environmental and Marine Sciences, University of Hull, Scarborough, YO11 3AZ, UK.

9 [2] School of Civil Engineering and Geosciences, Newcastle University, Newcastle upon Tyne, NE1

10 7RU, UK.

11 [3] School of Earth and Environment, University of Leeds, Leeds, LS2 9JT, UK.

12 [4] Department of Applied Biotechnology and Food Science, Budapest University of Technology and

13 Economics. 1111 Budapest, St. Gellért sq. 4. Hungary.

14

15

16 **Abstract**

17 This paper identifies the spatial extent of bauxite processing residue (red mud)-

18 derived contaminants and modes of transport within the Marcal and Rába river

19 systems after the dyke failure at Ajka, western Hungary. The geochemical signature

20 of the red mud is apparent throughout the 3076km^2 Marcal system principally with

21 elevated Al, V, As and Mo. Elevated concentrations of Cr, Ga and Ni are also

22 observed within 2km of the source areas in aqueous and particulate phases where

23 hyperalkalinity (pH <13.1) is apparent. While the concentrations of some trace

24 elements exceed aquatic life standards in waters (e.g. V, As) and fluvial sediments

25 (As, Cr, Ni, V), the spatial extent of these is limited to the Torna Creek and part of the

26 upper Marcal. Source samples show a bi-modal particle size distribution (peaks at 0.7

27 and 1.3 μm) which lends the material to ready fluvial transport. Where elevated

28 concentrations are found in fluvial sediments, sequential extraction suggests the bulk

29 of the As, Cr, Ni and V are associated with residual (aqua-regia/HF digest) phases and

30 unlikely to be mobile in the environment. However, at some depositional hotspots,

31 association of As, Cr and V with weak acid-extractable phases is observed.

32

33 **Introduction**

34 The dyke breach at the bauxite processing residue (red mud) depository at the Ajkai

35 Timfoldgyar Zrt alumina plant in Hungary on the 4th October 2010 released between

36 600,000 and 700,000m^3 of caustic red mud suspension[1]. While there have been other

37 notable examples of accidental release of caustic wastes to river systems[2,3], the Ajka

38 incident is unprecedented given the scale of the release and the type of material

39 involved. Immediate scientific efforts at the site have assessed the phytotoxicty of the

40 red mud given the vast areas (estimated to be 800ha)[4] of agricultural land inundated

41 and the public health risks associated with dust blows from the terrestrial deposits[5,6].

42

43 Red mud is the fine fraction by-product of alumina refining, of which between 70

44 million and 120 million tonnes are produced annually[4,7,8]. The specific composition

45 of red mud deposits, and their trace element constituent in particular, depends on the

46 quality of the bauxite ore from which they are enriched in the residue. The bulk

47 matrix of red mud typically comprises residual iron oxides (e.g. haematite), quartz,

48 sodium aluminosilicates, titanium dioxide, calcium carbonate/aluminate and sodium

49 hydroxide (which elevates pH up to 13)[5,9]. At Ajka, previous studies have highlighted

50 the presence of radionuclides (^{226}Ra, ^{232}Th and ^{40}K) in the deposits[7] and

51 characterisation studies soon after the spill highlighted elevated concentrations of V,

2

52   Cr, Ni and Co in two isolated red mud samples taken from deposits downstream of the

53   site[4]. Immediate studies on the bioavailability of potential trace contaminants to

54   plants suggest that trace contaminant availability (e.g. Cr, Co, Ni and V) is a

55   secondary issue compared to an elevated Na content of the material[4]. These findings

56   are consistent with other assessments undertaken on red mud deposits from sites

57   elsewhere globally[10] suggesting that the material, while enriched in various trace

58   elements, can be relatively benign. Indeed, multiple after uses for red mud have been

59   assessed in building materials[7] and as an environmental ameliorant[11]. Red mud and

60   derivative media have been shown to limit the mobility of many trace contaminants in

61   various contaminated land settings (e.g. mine sites) due primarily to sorption and co-

62   precipitation with the abundant ferric and aluminium oxides in the material[12-14].

63

64   Red mud leachates are hyperalkaline (pH 9-13) due to the NaOH digestant used in the

65   Bayer Process[15]. High pH itself in surface waters can be a source of direct toxicity to

66   aquatic life[16]. However, an equally important issue is the greater mobility of

67   oxyanionic trace elements such as As, Cr, Mo, V at elevated pH[17]. These

68   contaminants have been documented to occur in concentrations of 2-5mg L^{-1} at a

69   former mine pit lake in which red mud was dumped in western Poland[15]. Studies in

70   analogous hyperalkaline settings have also documented some of these elements

71   occurring at environmentally-significant concentrations, such as in waters draining

72   steel slag mounds[18], chromite ore residue sites[19] and fly ash disposal sites[20].

73

74   This paper presents an integrated assessment of water quality, contaminant transport

75   and fate in the water courses immediately downstream of the Ajka red mud disposal

76   site. Specific objectives of the work are to: (1) assess the impact, composition and

77 behaviour of residual aqueous releases from the disposal site, and (2) determine the

78 spatial extent and form of red mud-derived contaminants in the fluvial sediments

79 downstream of the site.

80

81 **Experimental section**

82

83 *Study site*

84 Sample locations along the course of the Torna Creek, Marcal, Rába and Mosoni-

85 Duna rivers are shown in Figure 1. Land cover across the catchments is dominated by

86 agriculture, with principal urban areas at Ajka, Pápa, and towards the confluence with

87 the Mosoni-Duna around the town of Győr. Bedrock geology in the upper catchment

88 is dominated by dolomites and limestones of Triassic age which lie beneath a

89 sequence of fluvial marls, slates and interbedded sands of Miocene age[1]. The Torna,

90 Marcal and Rába are all extensively channelised with levees minimising floodplain

91 extent, particularly downstream of Pápa (Figure 1).

92

93 *Water analyses*

94 Water and sediment samples were collected from the locations shown in Figure 1

95 under consistent low-to-moderate winter flow conditions on the 1st and 2nd December

96 2010 (mean daily flow at M4 was $11.5 m^3 s^{-1}$ on both days). Field data and water

97 samples were collected according to standard sampling protocols (see Supplementary

98 Information). Major anion concentrations were determined using a Dionex 100 Ion

99 Chromatograph and cation and minor element concentrations using a Perkin Elmer

100 Elan DRCII inductively Coupled Plasma-Mass Spectrometer (ICP-MS; for As, Cr and

101 Mo) and an Optima 5300 DV ICP-OES for all other elements quoted hereafter.

102

103 *Sediment samples*

104 At each station triplicate bulk (≈500g) sediment samples were collected by

105 aggregating three randomly collected sub-samples from a $12m^2$ area of stream bed (9

106 separate locations sampled at each reach to give three replicates). Additional spot

107 samples of transported red mud from floodplain deposits at Somlóvásárhely (S1)**,** fly

108 ash (that formed the disposal cell wall), stock-piled gypsum (used to dose waters in

109 the spill aftermath) and gypsum-affected fluvial sediments were taken at selected

110 sites. Sediments were homogenized, air-dried, disaggregated gently and sieved (2mm

111 aperture) prior to microwave-assisted total digestion (aqua regia and HF) following

112 standard methods[21]. Elemental concentrations in digests were analysed as per

113 aqueous trace element analyses. Selected dried and disaggregated samples from K1

114 and S1 were also prepared for SEM/EDS and particle size analysis. Sequential

115 extraction on combined triplicate samples from the sample stations was undertaken to

116 increase extractant solution/sediment ratio[22]. Extractant pH was checked after each

117 stage and conformed to standard values. All statistical analyses were undertaken in

118 Minitab v15. Data were not normally distributed even after log-transformation

119 (Kolmogorov-Smirnov $p>0.05$) so non-parametric methods were used. Principal

120 Component Analysis (PCA) was undertaken on standardized sediment element

121 concentration data.

122

123 **Results and Discussion**

124

125 *Major ion chemistry*

126   Reference samples (T2, M1) across the upper catchment are similar in composition,

127   being slightly alkaline, dominated by Ca-Mg-HCO$_3$ type, consistent with waters

128   draining from the Triassic dolomites (Table 1). Waters at site K1 characterise those

129   draining Cell X (Figure 1), which was the active cell at the western-most end of the

130   disposal site and contained fine-grained bauxite residue (red mud)[1]. The K1 waters

131   show characterise the leachate and red mud suspension pre-acid dosing, and show Na-

132   CO$_3$-OH dominated waters with hyperalkaline pH (13.1), low *Eh,* high suspended

133   solid content (13.3g L^{-1}) and high SO$_4^{2-}$ concentrations. The K1 site lies at the base of

134   a permeable reactive fly ash barrier (constructed using material from the dam wall),

135   built within two weeks of the accident across the dyke breach. Downstream of K1 the

136   waters are directed through a series of settlement lagoons and acid dosing units (HCl

137   and H$_2$SO$_4$) prior to the confluence of the northerly branch of the Torna Creek with its

138   southerly branch (Figure 1). The decrease in pH between K1 and K2 is explicable by

139   dilution of the waters from Cell X with uncontaminated waters on the northern branch

140   of the Torna Creek. Lagoons and check dams shortly downstream of K1 appear

141   effective in substantially reducing the suspended solid content of the water, while

142   further decreases in pH are apparent downstream (K3) due to acid dosing (Table 1).

143   While the drainage from K1 represents a significant point source of hyperalkaline

144   leachate to surface waters around the site, there are additional inputs of leachate from

145   Cell X into the southerly branch of the Torna Creek (just upstream of T1) via an acid

146   dosing unit (reflected in SO$_4^{2-}$ elevations above reference sites) to the south of Cell X.

147   The dilution of the contaminated water with progress downstream is reflected in

148   monotonic decrease in Na$^+$ and SO$_4^{2-}$ towards baseline concentrations, which are

149   achieved towards the confluence of the Rába and the Mosoni-Duna.

150

151 *Major and trace elements*

152 In hyperalkaline conditions at K1 numerous trace elements are elevated in both the

153 particulate and dissolved phase. Dissolved concentrations of Al, As, Cr, Ga, Mo, Ni,

154 Se, V and U (Table 1) are similar to those documented elsewhere[15]. Soluble

155 oxy(anionic) species are generally only detected in the northern branch of the Torna

156 Creek where pH remains elevated prior to acid dosing (Table 1, Figure S1) and

157 subsequent dilution at T1-T3. Cr, Ni, Se, and U concentrations decrease to baseline

158 (similar to reference site) levels or below detection limits by K3, due to changing

159 solubility with the decrease in pH (from 13.1 to 10.1)[17] and dilution. The trace

160 elements for which elevated concentrations in the water column are seen to propagate

161 furthest downstream are As, Mo and V (Table 1, Figure S1). These form oxyanions in

162 moderate to highly alkaline conditions and are a well-documented water quality issue

163 in waters draining high pH industrial residues[20,23]. In the circum-neutral pH, oxic

164 conditions downstream of K3, arsenic would be expected to be immobilised by

165 sorption or co-precipitation with both Hydrous Ferric Oxide (HFO) and oxides of

166 Al[24-25]for which numerous phases are predicted to be oversaturated around source

167 areas. Mass loading data highlights such rapid attenuation of dissolved As between

168 K3 and T3. Arsenic shows significant ($p<0.05$) positive correlation with particulate

169 Al, Ca and Ti (r_s=0.49-0.54) and no significant ($p<0.05$) correlation with Fe, which

170 may be a feature of consistently high Fe concentrations throughout the system from

171 both Ajka and natural lithogeneous sources.

172

173 At the water pH values measured the element V is predicted to be present principally

174 as vanadate (VO_4^{3-})[26] and analysis of fractions within the water column via sequential

175 filtration highlight a significant portion of V (typically 51-77%) being transported in

176   the dissolved phase around the source areas (K1-T3: Figure 2). The total loading of V

177   (Figure 2) stays relatively constant throughout the lower Torna and into the Marcal.

178   However, the proportion of particulate and colloidal V in particular, becomes more

179   important with distance down the Torna, suggesting sorption and/or (co-)precipitation

180   of dissolved V (Figure 2). There are strong and significant ($p<0.001$) correlations

181   between particulate V and all major particulate vectors (Al, Ca, Fe, Si, Ti; $r_s = 0.76$-

182   0.92) alluding to their importance in V attenuation and transport[27-28]. The total V

183   concentrations exceed recommended freshwater EQS[29] at the encountered hardness

184   from K1 to T3 at Devecser (5.2 km from source) suggesting that the elevated aqueous

185   V concentration is of relatively limited extent due primarily to dilution (given the

186   relatively consistent loading). Similar patterns are evident for Mo, with predominant

187   transport in the dissolved phase between K1 and K3 (Figure 2). The bulk sediment

188   analyses reports only moderate concentrations of Mo in the red mud samples (K1a-c:

189   11-18 mg kg^{-1}: Table 2), with peak concentrations in the fly ash itself (53 mg kg^{-1}).

190   Whether the enrichment of Mo in K1 waters is enhanced by the dissolution of Mo-

191   bearing phases at pH 13 in the fly ash[20] Permeable Reactive Barrier is uncertain. At

192   the pH values measured Mo is predicted to be predominantly present as the stable

193   molybdate oxyanion (MoO_4^{2-})[26] in the waters of the Torna Creek. With pH changes

194   downstream of K3, colloidal fractions subsequently dominate instream Mo loading,

195   which levels-off in the Torna before further increase in the Marcal. No significant

196   correlations ($p >0.05$) were apparent however for particulate Mo with any of the

197   major elements in particulate phase (Al, Ca, Fe, Si, Ti) although attenuation by oxides

198   and clays would be anticipated[29].

199

200 There is a rapid transition of Al from dissolved phase (at K1) to particulate phases at

201 T2 (Table 1). This is consistent with the decrease in pH along the north branch of the

202 Torna Creek. Particulate Al loading shows a marked decrease from peak

203 instantaneous loading of 1540kg d^{-1} downstream of K3 and T1 to less than half of that

204 at T6, suggesting significant instream attenuation via settlement of Al phases during

205 the Torna Creek (Figure 2). After the confluence with the Marcal, loading increases

206 again with increased stream competence. Loadings data through the Torna Creek

207 highlight a general trend of increase in Fe, Ti and Si loading downstream consistent

208 with suspended solids load trends. Particulate Ca loading curves show major gains

209 downstream of Kolontár and Devecser (T3) reflecting entrainment of both natural

210 fines and gypsum-amended substrates with increasing stream competence. Total

211 suspended sediment loading in the Torna Creek (Figure 2) highlights the increasing

212 transport of particulates with transit downstream of the site reflecting diffuse inputs

213 (e.g. runoff from red mud-inundated land), as well as entrainment of instream

214 sediments. This highlights the role of the Torna and upper Marcal catchment as a net

215 exporter of red mud-derived sediments under survey conditions.

216

217 *Bulk sediment analyses*

218 Table 2 presents mean bulk concentrations of major and trace elements in the fluvial

219 sediments. Of particular note in the source samples (K1) is enrichment of As, Ce, Co,

220 Cr, Ni, Pt, U, V and Zn (Table 2). All are at mean concentrations slightly higher than

221 initial reports[4] and of a similar order to sites elsewhere[30-31]. Similar concentrations are

222 reported at the S1 sample to those reported elsewhere after the spill[4] and are

223 consistent with the sampling location 10km downstream from the breach. Table 2 and

224 Figure 3 highlight a general decline in key red mud-associated trace elements (As, Cd,

225   Co, Cr, Ni and V) downstream from K1, albeit with several hotspots of enrichment

226   and some areas of preferential dilution. Low concentrations at K2 are a likely feature

227   of the extensive disturbance to flow paths and the ground-surface in the area close to

228   the source that has been a focus for remedial efforts. As such, K2 sediments show

229   enrichment of many indicators of drift deposits with elevated K and lower Al, Fe, Ti

230   and Ca concentrations. Moderately high concentrations of trace elements are visible

231   at T5 and T6 relative to upstream samples on Torna Creek. This may be a feature of

232   the reduced channelisation, lower gradient and resultant velocity in the lower reaches

233   of Torna Creek which lends itself to deposition of finer material. In the upper reaches

234   of the Marcal (T3-T4) trapezoidal cross-sections and straight planform are likely to

235   enhance entrainment of fine-grained spill deposits and encourage dilution of bed

236   sediments by uncontaminated, coarser sediments. Velocity data and suspended

237   sediment loading curves (Table 1, Figure 2) support this hypothesis.

238

239   Threshold Effects Levels (TEL) and Predicted Effects Levels (PEL) are widely used

240   as an initial screening tool for potential freshwater sediment toxicity[32]. Values are

241   presented in Table 2 for comparative purposes (and due caution in inferring mobility

242   must be heeded) and highlight the limited spatial extent of samples that exceed PEL

243   values, where prescribed. For Cr and Ni, concentrations well above PEL are apparent

244   at K1, K3, T1 and T5-6. While no formal TEL/PEL values are established for Co and

245   V, comparison with 'background'[32] levels suggest similar enrichment patterns to Cr

246   and Ni. It should also be noted that reference samples from urban settings (T2 from

247   Ajka) show elevations of Cr, Ni and V above respective background or TEL levels,

248   indicative of urban/industrial provenance for Cr, Ni and V in the sediments. Such

249   diffuse urban sources (e.g. highways runoff, manufacturing industries)[33] may also

250　account for the slight enrichment of Co, Cr, Cu, Ni and Zn in urban reaches of the

251　Rába and Mosoni-Duna (samples R2 and MD1, Table 2).　Cd samples only show

252　significant enrichment above PEL values at site K1. Arsenic enrichment is apparent in

253　source samples and on the Marcal at downstream stations M5 and M9 (Figure 3).

254

255　PCA analysis (Figure 4) highlights the key indicators of the red mud in the fluvial

256　sediments and shows the mixing gradient with progression through the Torna Creek,

257　Marcal, Rába and Mosoni-Duna Rivers.　Reference sediments (R1, T2, M1) are

258　indicated by elevated Ba, Mg and K relative to red mud contaminated sediments and

259　indicative of lithogeneous weathering (dolomites and drift deposits[1]).　PCA axis 1

260　shows the rapid dilution of red mud from K1 through Torna Creek, with occasional

261　red mud-enriched samples from the upper Marcal (M2). The second axis is

262　characterised by the Ca-rich, gypsum-amended substrates in the lower Marcal (M11),

263　which plots close to the fly ash sample from the dam wall given similar Ca content.

264　Gypsum dosing of stream waters took place from Kolontár to Rábaszentmihály

265　(Figure 1) at bridge crossings and stream access points to neutralise waters[6].

266

267　Sequential extraction data (Figure 3) show the majority of potential contaminants in

268　the HF/aqua-regia step. This supports interpretation of previous site data with regard

269　the relatively limited potential bioavailability of many trace elements[4].　High Al

270　concentrations in the residual fraction are apparent in both undisturbed and impacted

271　samples. Enrichment of Al in the NaOAc and $NH_2OH.HCl$ steps is apparent in source

272　samples and suggests reasonable quantities of Al that could be transformed in suitable

273　redox settings. While significant inventories of Fe are associated with the

274　$NH_2OH.HCl$ step (800-3300mg kg^{-1}), they represent only a fraction of the total Fe

275   concentration, which is largely present as stable, well-crystallised, residual phases,

276   such as haematite which is usually extracted in step $5^{5,34}$. Cr, Co and Ni show broadly

277   similar patterns with residual phases predominant, similar to patterns reported at other

278   sites[31]. H_2O_2 and $NH_2OH.HCl$ extracts contain increasing concentrations of Ni and

279   Co downstream, while a small number of the heavily-red mud impacted sediments

280   (e.g. K3, T1, T6, M1) report moderate Cr inventories in weakly extractable phases

281   such as amorphous Fe/Mn oxides and carbonates. For the more mobile elements in the

282   aqueous phase (As, Mo and V), greater proportions are found in non-residual phases

283   in transported samples in the lower Torna Creek and upper Marcal. A significant

284   portion of V is associated with the $NH_2OH.HCl$ extraction (16-60%) in samples

285   downstream of source areas, while between 22 and 77% of Mo is associated with this

286   fraction, suggesting the importance of oxides in attenuation of Mo and V. The

287   importance of residual phases declines for As from source material (90%) with

288   progress downstream (minimum of 24% at M11). Concentrations of As in the

289   NaOAc and $NH_2OH.HCl$ extraction phases reach up to 26mg kg^{-1} at M7. These

290   patterns for As, Mo and V are likely to reflect instream attenuation processes (e.g.

291   sorption to readily-extractable Fe, Al oxides and carbonate phases) during transit

292   through the system, through which dissolved loads typically decline (Figure 2).

293

294   *SEM and particle size analysis*

295   SEM analysis (Figure 6) of source material (sample K1) highlights predominant fine

296   grained material (<4μm in diameter) which follows a bi-modal distribution

297   comprising: (1) larger, plate-like particles (diameter typically 1-6μm), and (2) finer,

298   more rounded particles of diameter 50-100nm typically forming as aggregates up to

299   1μm in size. The former are rich in Al, Si and Na with significant Ca, S, Fe and Ti

300 (Supplementary Information), consistent with cancrinite which has been identified

301 elsewhere in samples from the site[5]. EDS spectra from the finer fractions shows

302 consistent enrichment with Fe and O indicative of iron oxide phases (e.g. haematite)

303 being largely hosted in these smaller particles. These nano-particulate aggregates are

304 likely to be driving the observed pattern of increasing suspended solid loading

305 through the Torna Creek and Marcal River and are likely to be readily entrained even

306 under low velocities. Analysis of transported floodplain samples (S1) shows an

307 additional group of particles 10-40µm in diameter indicative of entrainment of

308 uncontaminated surface sediments (hence dilution of total concentrations at S1) in the

309 downstream floodplain deposits (Figure 6).

310

311 *Implications for system recovery*

312 The particularly fine-grained nature of the contaminant-bearing phases in red mud is

313 in contrast to most river systems impacted by accidental contaminant release. Most

314 examples of tailings failure concern metalliferous, acidic and/or cyanide-rich

315 materials, where sediment-borne contaminants are concentrated in fractions of the

316 order of 10-500µm[35] and the signal of metal contamination remains in the river system

317 several years after the spill[36]. The data from this study suggests that within-channel

318 storage of large inventories of red mud appears to be relatively limited in extent. Even

319 where moderately high concentrations of trace elements (e.g. As, Cr, V) are reported,

320 they are predominantly associated with residual phases suggesting limited potential

321 mobility in the environment. At some depositional hotspots, association of As, Cr and

322 V with weak acid and oxalate extractable phases gives scope for some future mobility

323 and should be the focus for longer-term study. Given the volume of material that was

324 released from the impoundment and the relatively low gradient of the river system

downstream of Ajka (mean gradient of 0.93m km^{-1}), the rapid dilution of sediment-borne contaminants is encouraging and likely to reflect the preferential transport out of the system of the <10µm fractions that characterise the released material.

Supporting Information Available

Detailed methods, EDS spectra, contaminant correlation and mineral phase data are available in Supplementary Information.

References

[1]Reeves, H.J.; Wealthall, G.; Younger, P.L. Advisory visit to the bauxite processing tailings dam near Ajka, Vesprém County, western Hungary. British Geological Survey, Keyworth, UK. Open Report OR/11/006. 2011.

[2]Cairns, J.; Dickson, K.L.; Crossman, J.S. The biological recovery of the Clinch River following a fly ash pond spill. In *25th Industrial Waste Conference Proceedings*. Purdue University, West Lafayette, Indiana, USA. pp.182-192. 1972.

351   [3]Younger, P.L.; Banwart, S.A.; Hedin, R.S. *Mine water: hydrology, pollution, remediation.*

352   Kluwer Academic Publishers, Holland. 2002.

353   [4]Ruyters, S.; Mertens, J.; Vassilieva, E.; Dehandschutter, B.; Poffijn, A.; Smolders, E. The red

354   mud accident in Ajka (Hungary): Plant toxicity and trace metal bioavailability in red mud

355   contaminated soil. *Environ. Sci. Technol.* **2011**. *45,* 1616-1622.

356   [5]Gelencsér, A.; Kováts, N.; Turóoczi, B.; Rostási, Á.; Hoffer, A.; Imre, K.; Nyirő-Kósa, I.;

357   Csákberényi-Malasics, D.; Tóth, Á.; Czitrovsky, A.; Nagy, A.; Nagy, S.; Ács, A.; Kovács,

358   A.; Ferincz, Á.; Hartyáni, Z.; Pósfai, M. The red mud accident in Ajka (Hungary):

359   characterization and potential health effects of fugitive dust. *Environ. Sci. Technol.* **2011**.

360   *45*, 1608-1615.

361   [6]Gruiz, K. *Environmental Information: The red mud catastrophe in Hungary.*

362   http://enfo.agt.bme.hu/drupal/en/gallery/8081 2010.

363   [7]Power, G.; Gräfe, M.; Klauber, C. *Review of current bauxite residue management, disposal*

364   *and storage: practices, engineering and science*. CSIRO Document DMR-3608. 2009.

365   [8]Palmer, S.J.; Frost, R.L.; Nguyen, T. Hydrotalcites and their role in coordination of anions in

366   Bayer liquors: anion binding in layered double hydroxides. *Coordination Chemistry*

367   *Reviews.* **2009**. *253,* 250-267.

368   [9]Somlai, J.; Jobbágy, V., Kovács, J., Tarján, S., Kovács, T. Radiological aspects of the

369   usability of red mud as building material additive. *J. Hazard. Mater.* **2008**. *150***,** 541-545.

370   [10]Courtney, R.G.; Timpson, J.P. Reclamation of fine fraction bauxite processing residue (red

371   mud) amended with coarse fraction residue and gypsum. *Water, Soil, Air Pollut.* **2005**. *164,*

372   91-102.

373   [11]Zijlstra, J.J.P.; Dessì, R.; Peretti, R.; Zucca. A. Treatment of percolate from metal sulphide

374   mine tailings with a permeable reactive barrier of transformed red mud. *Water Environ.*

375   *Res.* **2010**. *82*, 319-327.

376   [12]Feigl, V.; Uzinger, N.; Gruiz, K. Chemical stabilisation of toxic metals in soil microcosms.

377   *Land Contam. Reclam.* **2009**, *17,* 485–496.

378   [13]Munro, L.D.; Clark, M.W.; McConchie. D. A Bauxsol[TM]-based permeable reactive barrier

379   for the treatment of acid rock drainage. *Mine Water Environ.* **2004**, *23*, 183-194.

380   [14]Khaitan S.; Dzombak D.A.; Lowry G.V. Neutralization of bauxite residue with acidic fly

381   ash. *Environ. Eng. Sci.* **2009**. *26*, 431-440.

382   [15]Czop M.; Motyka J.; Sracek, C; Szuwarzynski, O. Geochemistry of the hyperalkaline Gorka

383   Pit Lake (pH>13) in the Chrzanow Region, Southern Poland. *Water, Air Soil Pollut.* **2011**.

384   *214***,** 423-434.

385   [16]Wilkie, M.P.; Wood, C.M. The adaptations of fish to extremely alkaline environments.

386   *Comparative Biochemistry and Physiology,* **1996**. *113B*, 665-673.

387   [17]Langmuir, D. *Aqueous Environmental Geochemistry*: Prentice-Hall, NJ, USA. 1997

388   [18]Mayes, W.M.; Younger, P.L.; Aumônier, J. Hydrogeochemistry of alkaline steel slag

389   leachates in the UK. *Water, Air Soil Pollut.* **2008**. *195*, 35-50.

390   [19]Stewart, D.I.; Burke, I.T.; Hughes-Berry, D.V.; Whittleston, R.A. Microbially-mediated

391   chromate reduction in soil contaminated by highly alkaline leachate from chromium

392   containing waste. *Ecol. Engineering.* **2010**. *36*, 211-221.

393   [20]Cornelis, G.; Johnson, C.A.; Van Gerven, T.; Vandecasteele, C. Leaching mechanisms of

394   oxyanionic metalloid and metal species in alkaline solid wastes: a review. *App. Geochem.*

395   **2008**, *23*, 955-976.

396   [21]USEPA (1996) Microwave assisted acid digestion of siliceous and organically based

397   matrices. USEPA Method 2052. 1996

398   [22]Rauret, G.; Rubio, R.; Lopez-Sanchez, J.F. Optimization of Tessier Procedure for Metal

399   Solid Speciation in river sediments *Int. J. Environ. Anal.Chem.***1989**, *36*, 69-83.

400   [23]Fällman, A-M. Leaching of chromium and barium from steel slag in laboratory and field

401   tests – a solubility controlled process? *Waste Management.* **2000**. *20,* 149-154.

402   [24]Gupta S.K.; Chen, K.Y. Arsenic removal by adsorption. *J. Water Pollut. Control Fed.* **1978**.

403   *50*, 493-506.

404   [25]Dzombak D.A.; Morel, F.M.M. *Surface Complexation Modelling: Hydrous Ferric Oxide.*

405   Wiley-Interscience. NY, USA. 1990.

406   [26]Takeno, N. *Atlas of Eh-pH diagrams: intercomparison of thermodynamic databases.*

407   Geological Survey of Japan Open File Report no. 149. 2005.

408   [27]Naeem A.; Westerhoff, P.; Mustafa, S. Vanadium removal by metal (hydr)oxide adsorbents.

409   *Water. Res.* **2007**. *41*, 1596-1602.

410   [28]Wällstedt, T.: Björkvald, L.; Gustafsson, J.P. Increasing concentrations of arsenic and

411   vanadium in (southern) Swedish streams. *App. Geochem.* **2010**. *25*, 1162-1175.

412   [29]Goldberg, S.; Forster, H.S.; Godfrey, C.L. Molybdenum adsorption on oxides, clay minerals

413   and soils. *Soil Sci. Soc. Am. J.* **1996**. *60*, 425-432.

414   [30]Khaitan S.; Dzombak D.A.; Lowry G.V. Chemistry and acid neutralization capacity of

415   bauxite residue. *Environ. Eng. Sci.* **2009**. *26*, 873-881.

416   [31]Ghosh, I.; Guha, S.; Balasubramaniam, R,; Kumar, A.V.R. Leaching of metals from fresh

417   and sintered red mud. *J. Hazard. Mater.* **2011**, *185,* 662-668.

418   [32]Buchman, M.F. *NOAA Screening Quick Reference Tables*, NOAA HAZMAT Report 99-1,

419   Seattle WA. Coastal Protection and Restoration Division, National Oceanic and Atmospheric

420   Administration, 12pp. 1999.

421   [33]Westerlund, C.; Viklander, M.; Bäckström, M. Seasonal variations in road runoff quality in

422   Luleå, Sweden. *Water Sci. Technol.* **2003**. *48,* 93-101.

423   [34]Xiao-Quan, S; Bin, C. Evaluation of sequential extraction for speciation of trace metals in

424   model soil containing natural minerals and humic acid. *Anal. Chem.* 1993. **65**, 802-807.

425   [35]Hudson-Edwards, K.A.; Macklin, M.G.; Jamieson, H.E., Brewer, P.A.; Coulthard, T.J.;

426   Howard, A.J.; Turner, J.N. The impact of tailings dam spills and clean-up operations on

427   sediment and water quality in river systems: the Ríos Agrio–Guadiamar, Aznalcóllar, Spain.

428   *App. Geochem.* **2003**. *18*, 221-239.

429   [36]Macklin, M.G.; Brewer, P.A.; Balteanu, D.; Coulthard, T.J.; Driga, B.; Howard, A.J.;

430   Zaharia, S. The long term fate and environmental significance of contaminant metals released

431   by the January and March 2000 mining tailings dam failures in Maramures County, upper

432   Tisa Basin, Romania. *App. Geochem.* **2003**. *18*, 241-257.

433
434

435 Table 1. Hydrochemical composition of the waters in the Torna Creek and upper
436 Marcal on 1/12/10. Data present total values with filtered (0.45μm filter) data in
437 parenthesis. '<' denotes values below the given limit of detection.
438
439

Determinand	T2	K1	K2	K3	T1	T3	T4	T5	T6	M1
pH	8.30	13.06	10.50	10.08	8.40	8.34	8.46	8.71	8.60	8.31
Temperature (^{o}C)	2.8	3.6	4.2	3.9	5	3.3	2.6	1.3	1.6	0.7
Specific conductance (μS cm^{-2})	825	162900	3597	1715	1448	1505	1175	1076	966	911
ORP (V)	0.125	0.023	0.057	0.003	0.033	0.054	0.040	0.038	0.111	0.106
Mean velocity (m s^{-1})	0.81	<0.01	0.76	0.21	1.27	1.70	1.04	0.90	0.65	-
Major ions / elements mg L^{-1}										
Ca	143 (138)	1515 (1.3)	89.13 (16.86)	37.50 (15.21)	213.08 (198.99)	184.91 (175.02)	169.30 (161.52)	140.51 (134.22)	136.76 (132.91)	121.31 (120.80)
Mg	37 (36)	9.7 (0.001)	21.92 (13.29)	12.48 (9.02)	53.11 (50.58)	45.52 (44.56)	39.45 (39.07)	38.78 (38.38)	36.62 (36.39)	41.27 (41.36)
K	5 (5)	115 (85)	35.24 (35.60)	35.14 (35.24)	8.33 (8.04)	11.10 (11.39)	8.45 (8.43)	8.68 (8.64)	7.25 (7.15)	7.55 (7.69)
Na	13 (12)	(701)	374.15 (369.12)	393.90 (392.73)	68.42 (67.25)	139.38 (137.57)	79.10 (78.37)	79.59 (79.10)	52.85 (52.14)	24.30 (24.34)
Al	0.2 (0.01)	1228 (659)	18.19 (11.63)	12.73 (9.02)	9.96 (0.25)	9.83 (0.37)	4.01 (0.41)	3.75 (0.64)	1.88 (0.23)	0.22 (0.04)
Cl	25	83	49.70	116	34.60	110	50.90	47.20	37	31.20
SO$_4$	67	727	283	260	363	321	256	185	154	97.40
Total Alkalinity	340	7160	570	440	342	334	300	348 (316)	298 (296)	346 (340)
OH calculated		1125.8	1.10							
CO$_3$ calculated		2445.8	248							
HCO$_3$ calculated	414.80	1.40	165.20	536.80	417.24	407.48	366.00	424.56	363.56	422.12
Suspended solids	49.6	13260	490.0	208.0	139.6	105.6	82.0	87.6	70.8	0.4
Trace elements (μg L^{-1})										
As	<0.1	3926 (3612)	224 (156)	181 (147)	108 (29)	124 (1)	43 (4)	37 (4)	33 (4)	<0.1
B	<2	1009 (900)	30 (30)	<2	<2	<2	<2	<2	<2	<2
Ba	50 (46)	297 (1)	34 (3)	14 (3)	45 (33)	39 (23)	39 (27)	39 (27)	41 (33)	47 (45)
Be	<0.1	46 (<0.1)	<0.1	<0.1	<0.1	<0.1	<0.1	<0.1	<0.1	<0.1
Cd	<0.1	59 (53)	3 (<0.1)	<0.1	<0.1	2 (<0.1)	<0.1	<0.1	<0.1	<0.1
Co	<1	17 (<1)	<1	<1	<1	<1	<1	<1	<1	<1
Cr	<0.1	356 (49)	1.2 (0.9)	5.8 (4.5)	8.7 (5.6)	6.6 (4.3)	1.4 (<0.1)	4.6 (<0.1)	1.0 (<0.1)	<0.1
Cu	3 (2)	390 (310)	15 (9)	18 (14)	5 (2)	5 (3)	4 (2)	4 (2)	3 (2)	2 (2)
Fe	346 (<10)	10212 (<10)	1080 (<10)	610 (<10)	760 (<10)	380 (<10)	360 (<10)	430 (<10)	500 (<10)	150 (<10)
Ga	12 (11)	2350 (2340)	129 (120)	122 (117)	79 (31)	72 (39)	47 (35)	40 (37)	22 (19)	18 (<1)
Li	4 (4)	303 (27)	215 (213)	197 (197)	22 (19)	37 (36)	20 (20)	20 (18)	13 (13)	8 (7)
Mn	84 (39)	9894 (<1)	130 (3)	77 (8)	208 (67)	205 (87)	161 (81)	175 (86)	210 (86)	29 (20)
Mo	19 (11)	5443 (4114)	405 (398)	420 (416)	77 (74)	155 (152)	83 (78)	93 (77)	58 (44)	13 (11)
Ni	5 (<1)	267 (36)	6.7 (4.5)	6.9 (4.6)	9.0 (6.0)	8.6 (6.1)	7.6 (5.9)	8.6 (4.5)	9.1 (5.8)	1.8 (1.4)
Pb	12 (2)	<1	0.00 (0.01)	<1	<1	<1	2 (<1)	7 (<1)	4 (<1)	<1
Si	3389 (3211)	499248 (668)	4473 (1524)	2635 (1044)	3808 (2885)	3644 (2588)	3077 (2110)	3062 (2052)	3206 (2609)	3099 (2884)
Sr	251 (241)	8819 (2)	334 (153)	165 (107)	909 (848)	755 (711)	582 (557)	553 (528)	512 (500)	509 (499)
V	<1	6398 (5709)	334 (323)	347 (343)	66 (26)	103 (60)	48 (39)	47 (41)	35 (30)	<1
W	<5	510 (483)	19 (10)	19 (9)	<5	<5	<5	<5	<5	<5
Zn	13 (10)	446 (49)	20 (2)	8 (1)	27 (14)	21 (16)	23 (13)	16 (10)	13 (10)	21 (19)

Table 2. Mean composition of digested fluvial sediments (*n*=3) at selected sample stations on the Torna Creek and Marcal River. All values in mg kg^{-1}. Reference samples M1 and T2 shown on right hand side (italics). FA: fly ash from impoundment wall, S1: floodplain deposit from Somlóvásàrhely. Sb and Se below detection limits of 0.1 mg kg^{-1}.

Element	K1	FA	K2	K3	T1	T3	T4	S1	T5	T6	M2	*M1*	*T2*	TEL (PEL)[a]
Ca	53501	156762	107091	79138	79910	88713	82587	47909	73069	67855	62944	17083	40409	
Mg	2982	10336	16105	7111	8733	10650	8831	3674	7718	6741	6045	3859	10534	
K	737	1365	10148	5543	5476	7056	6025	2637	5239	4634	4170	8166	9235	
Na	39918	2782	6630	19391	21980	16000	19123	43224	26116	29488	32942	5350	9522	
Fe	210265	16558	37398	113480	141564	48123	30841	174425	29266	81109	80965	11142	13055	
Al	75160	20132	48407	56318	59628	54785	56910	65307	59001	60406	61571	22829	27292	
Si	27925	26544	91417	75909	65084	77470	72821	47717	66002	62180	58633	339271	54682	
As	78.5	29.9	32.3	51.9	54.3	46.2	50.8	61.3	52.8	54.9	56.3	5.8	1.7	5.9 (17)
Ba	59.8	18.6	174.7	168.4	134.3	159.1	153.9	52.0	121.7	109.2	94.3	183.7	163.9	0.7*
Be	9.1	0.6	1.8	4.6	5.6	1.9	1.2	7.3	1.7	3.5	3.2	0.8	<0.1	
Cd	4.0	<0.1	0.6	1.7	2.1	1.5	1.8	2.7	2.0	2.1	2.3	0.3	0.1	0.6 (3.5)
Ce	473.2	8.4	66.4	254.8	264.8	195.3	238.3	422.5	285.4	315.4	341.1	25.5	27.5	
Co	97.1	4.9	13.0	52.4	54.1	39.8	48.8	85.3	58.0	64.0	69.1	6.0	8.5	10*
Cr	810.7	43.6	84.4	372.6	422.6	293.2	362.8	592.8	416.3	457.3	488.8	30.3	29.2	37.3 (90)
Cu	60.3	14.9	18.4	42.6	40.5	33.8	39.0	47.6	40.1	42.2	43.3	9.3	15.1	35.7 (197)
Ga	79.3	16.6	28.2	52.9	53.4	44.8	50.4	69.0	54.7	58.0	60.6	8.9	13.0	
Li	57.5	30.1	46.6	60.5	54.9	54.0	56.5	65.3	58.6	60.1	61.4	12.7	13.6	
Mn	2565.8	182.0	443.6	1606.8	1538.7	1196.4	1447.3	2462.3	1702.0	1870.5	2011.6	292.8	420.8	400*
Mo	14.4	53.0	8.8	7.3	10.1	8.7	8.7	11.2	9.5	9.8	10.2	7.7	5.4	
Ni	291.7	26.8	28.3	140.7	153.5	107.5	133.9	246.0	162.5	180.8	196.4	12.5	7.6	18 (35.9)
Pb	79.8	1.8	3.5	39.6	41.0	28.0	36.2	68.1	44.1	49.5	53.9	1.3	2.6	35 (91.3)
Sr	290.2	375.7	214.9	235.0	246.7	232.2	237.9	299.1	256.4	264.5	273.3	91.5	124.3	49*
Ti	24848.2	1249.2	3435.1	12415.5	15073.5	5456.9	4764.7	21474.5	3721.8	9707.5	8019.3	1692.2	3665.2	
U	338.5	57.6	36.9	156.9	177.5	123.8	152.7	247.1	174.6	191.5	204.4	<0.5	2.1	
V	891.2	185.6	114.8	458.9	488.3	354.0	433.7	743.2	510.3	562.4	605.3	28.9	34.4	50*
Zn	173.2	29.2	58.5	104.3	112.0	91.6	102.7	132.0	108.8	114.5	118.4	26.3	26.6	123 (315)
Zr	628.9	21.2	72.2	323.1	341.4	245.5	303.3	531.8	360.2	398.4	430.2	18.4	35.1	

[a]TEL: Threshold Effects Level; PEL: Predicted Effects Level, *: 'Background' level. All for freshwater sediments[32]
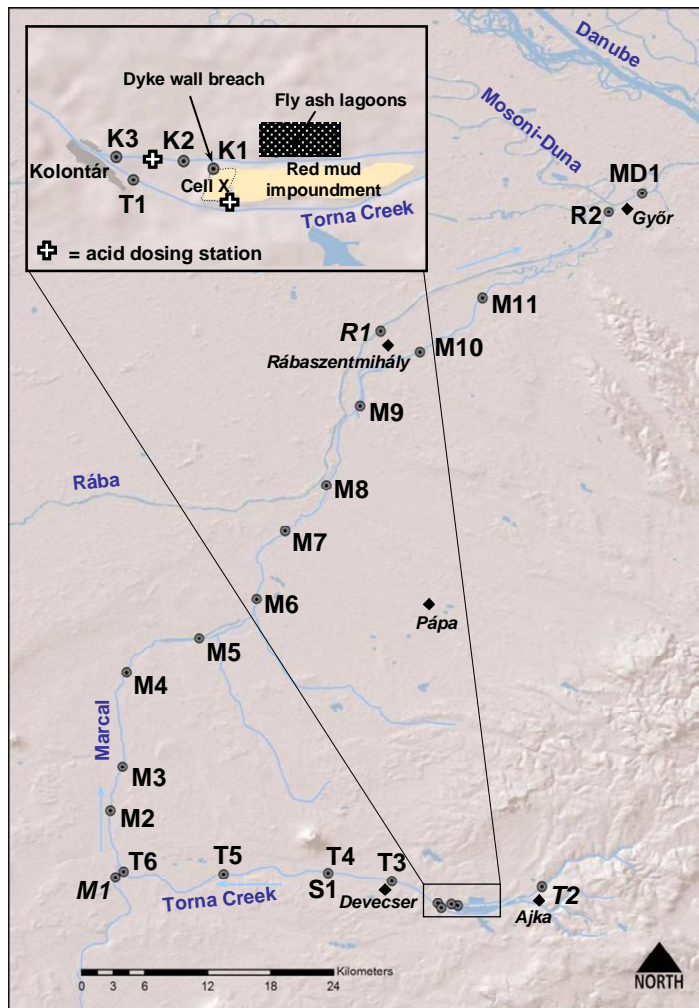
Figure 1. Location map of sample stations (circles). Centres of population shown with diamond. Reference site labels in italics.
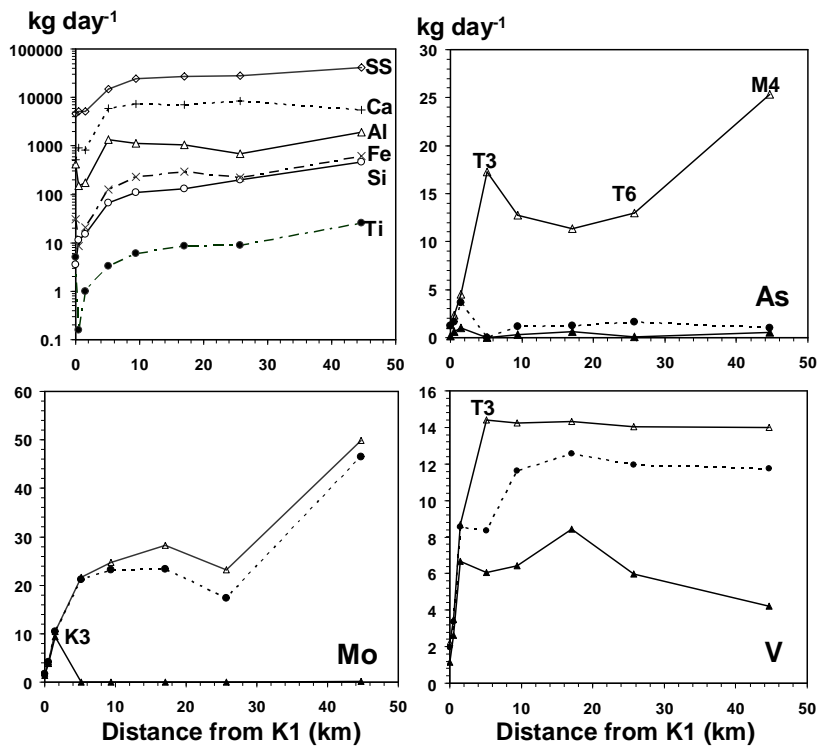
Figure 2. Partitioning of load (kg day^{-1}) of selected metals and metalloids with distance downstream of the dyke breach alongside suspended solid loading (kg day^{-1}). Particulate loading for major elements only shown in upper left image alongside suspended solids (SS). Note also logarithmic y axis on upper left image. All other images show total loading (Δ marker with solid black line), filtered (0.45μm) loading (● marker with dashed black line) and dissolved (passes 10kDa centrifuge filter) loading (▲ marker with solid black line).
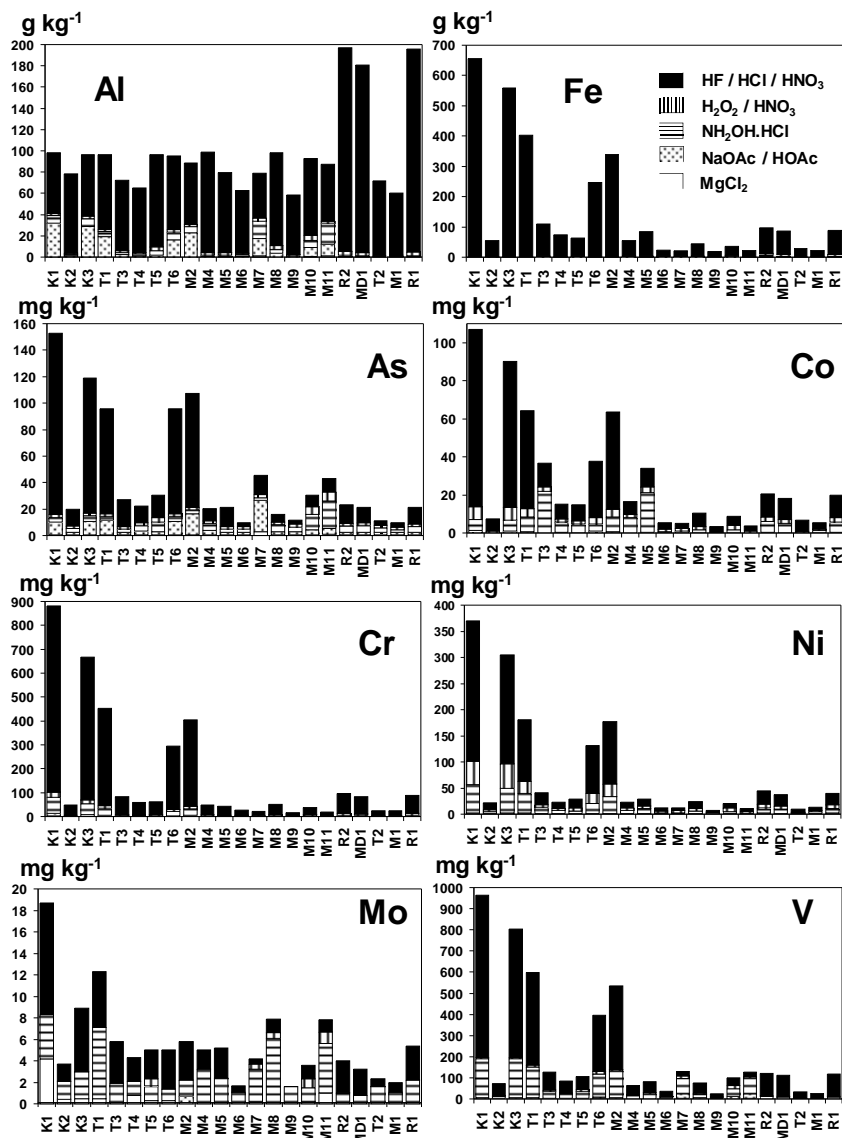
Figure 3. Sequential extraction of selected major and trace elements in stream sediment samples in the Marcal, Rába and Mosoni-Duna rivers.
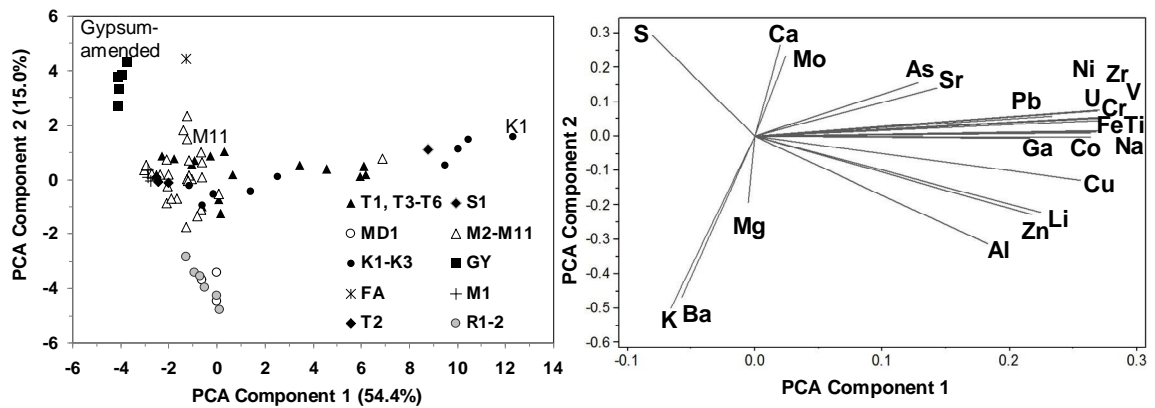
Figure 4. PCA of total fluvial sediment elemental concentrations in the studied rivers. Figures show PCA bi-plot by site (left image) and with eigenvectors for analysed elements (right image).
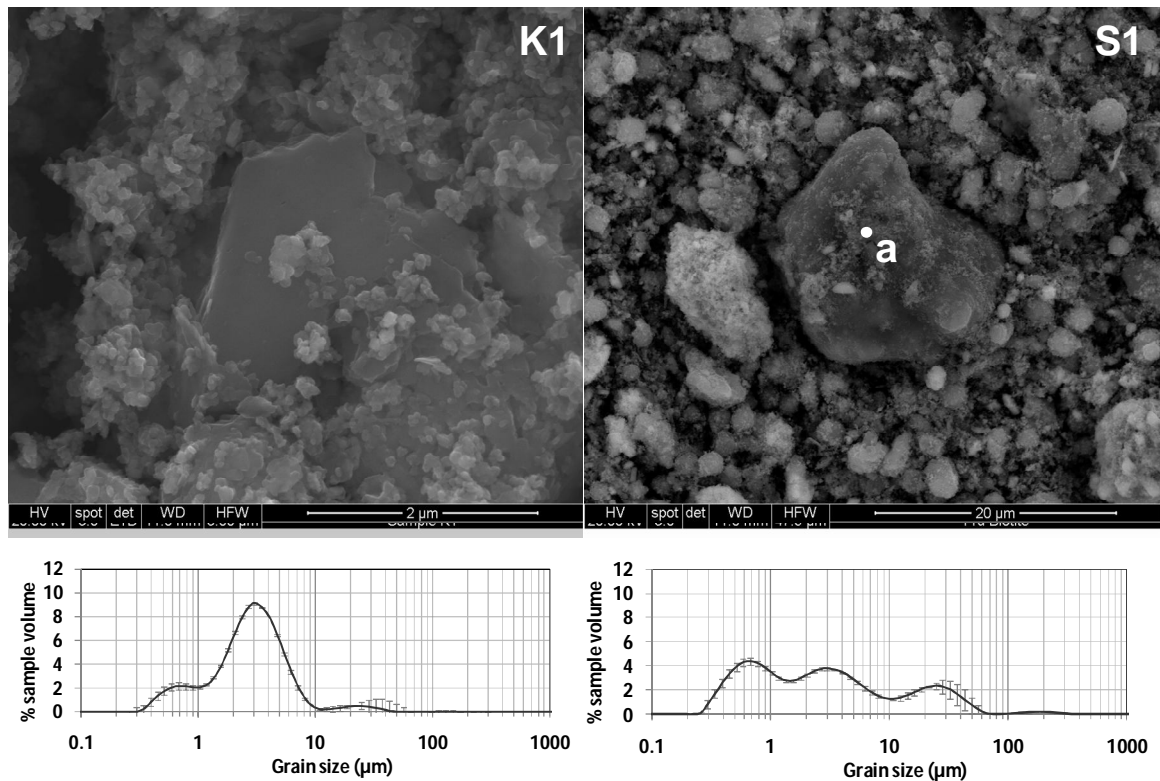

Figure 5. SEM and particle size distribution of samples K1 (source material) and S1 (transported red mud). EDS spectra for point 'a' in Supplementary Information.